

Sensory Flux from the Eye: Biological Sensing-of-Sensing (Veillametrics) for 3D Augmented-Reality Environments

Ryan Janzen and Steve Mann
Department of Electrical and Computer Engineering
University of Toronto

Abstract—We measure and visualize the ability-to-see, from the human eye, as that ability-to-see propagates through space. “Biological veillance flux” is a metric of sensory precision emitted from the eyes and falling on objects, with much greater detail than merely tracking the center of the eye’s field of view.

This work makes it possible to “see sight” and “measure sight” as the “sight” travels through three-dimensional space. In earlier work we measured veillance flux from electronic sensors and cameras. Now, we examine biological veillance flux. The result is a method to detect radiation of information-bearing optical sensitivity, as opposed to radiation of ordinary light energy in the opposite direction.

These measurements can be used as an augmented-reality visualization of human sight. They can serve as an interactive score tracking how much a target is seen. Additionally, they could serve as a data-rich metric of visual precision directed by human eyes toward control panels in industrial applications, or as a metric of visual precision directed by human eyes towards printed material or digital media, for advertising, arts or entertainment applications. Extramissive optics, as a new field of research, is thus expanded into the biological realm.

I. INTRODUCTION

The new concepts of a *veillance field* and *veillance flux* have been introduced as a mathematical formulation to account for the *ability to sense* as it propagates through space from a sensor [1].

An intersecting web of veillance field lines and veillance flux, ordinarily hidden in the world around us, are “emitted” by various cameras mounted to buildings, handheld and body-worn cameras, and embedded vision on hands-free doors, faucets, and lighting systems. Veillance is also “emitted” by other sensors, such as microphones and thermostats [1][2].

The first measurements of the veillance field employed a laser-scanning method, to quantify the ability to see, and its absorption, reflection and refraction as it propagated through space from cameras [1]. The veillance field of electronic cameras has also been sensed by an inverse-radiation dosimeter [2], which detects how much veillance “dose” an individual is exposed to—*i.e.* how much he/she was photographed or otherwise sensed. 3D visualizations of veillance flux, streaming out of electronic cameras, can now be seen by wearing augmented reality glasses, so the veillance flux is graphically overlaid on a moving 3D environment [3]. The veillance field also exists for sound wave sensing, atmospheric pollution



Fig. 1. Output rendering of biological veillance flux from a human test subject. The veillance flux was first tested and measured by an algorithm described in this paper. Finally a rendering was generated showing the sensitivity-to-light as it propagates through space. This rendering has veillance flux mapped to a color space, compensated for $1/r^2$ radiative decay.

sensing, weather and climate sensing, fluid thermal sensing, *etc.* [1]. This sensing-of-sensing is also called *veillametrics*, *metasensing*, and *extramissive optics*. New research results are made possible by being able to test and measure sensing itself.¹

In this work, we “see sight” of biological systems, for the first time. Industrial and medical applications come from this 3D sight map – a data-rich metric of what objects (road signs, control panels, advertisements) are seen by a human – much more precisely than by merely tracking eye motion.

A novel eye test now produces an intricate, data-rich map of the ability-to-see which moves through 3D space, “emitted” from the eyes, refracting through eyeglasses, reflecting around rooms, and precisely measured at various points in space. By measuring “sight”, we can measure, see, and experience that which is invisible: the capacity-to-sense itself.

¹We originally proposed *veillametrics* for measuring any manmade sensor. In our previous paper [2], as an aside we showed an early mockup of *bio-veillametrics*, to allude to preliminary work being started on this project. In this paper we fully present the technical details of this research, including a novel algorithm for dynamically testing biological organisms’ veillance fields.

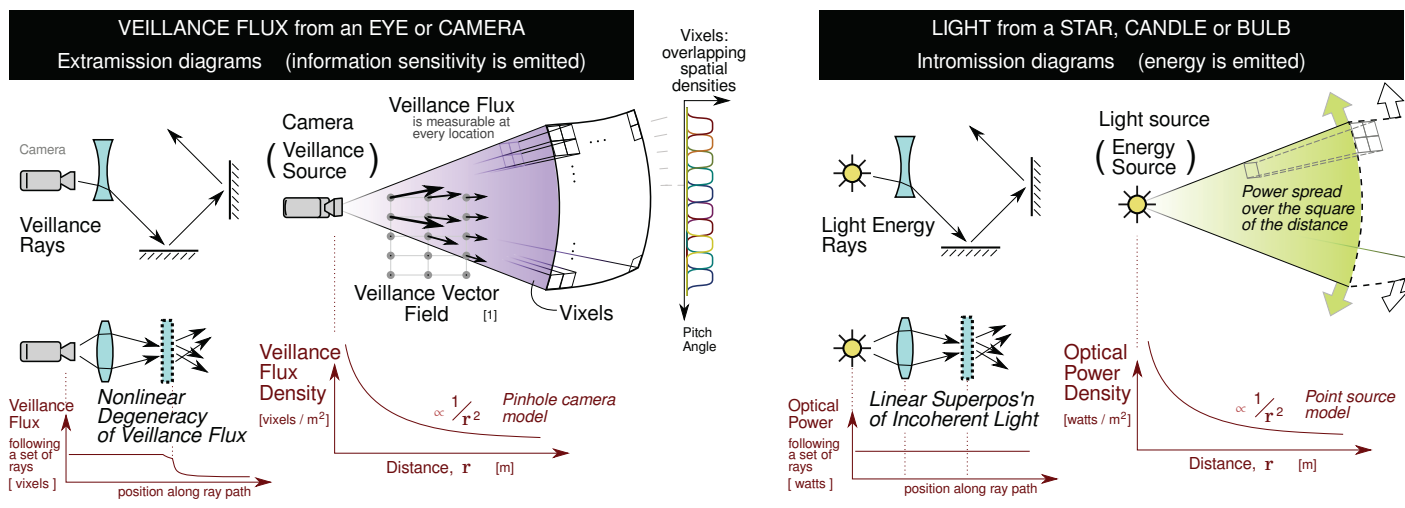
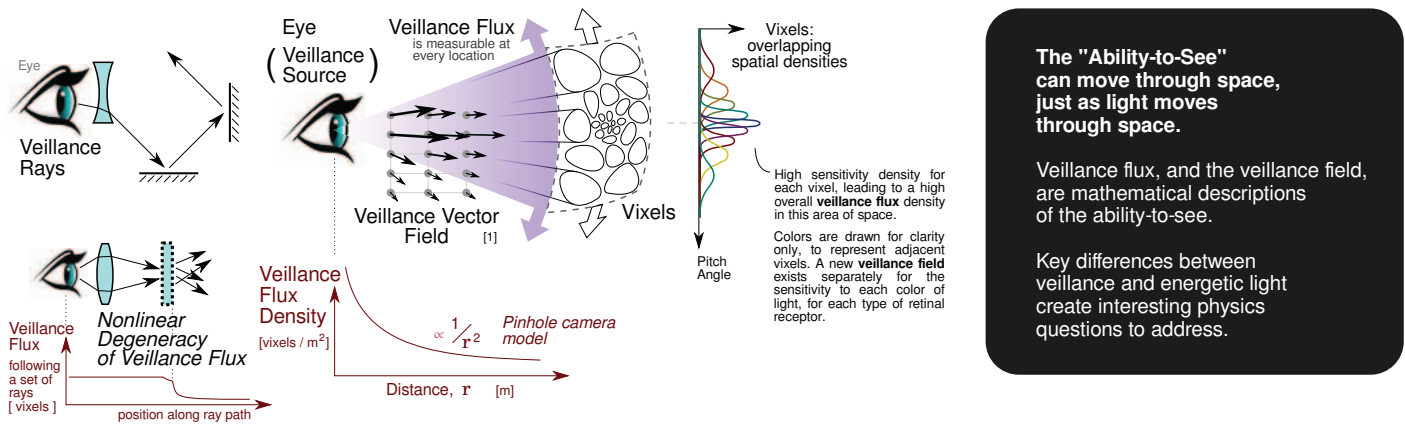


Fig. 2. Extramission diagrams of veillance propagation, v.s. Intromission diagrams of light propagation.

II. BACKGROUND: SEEING AND MEASURING SIGHT

Early veillametrics [1][2], were able to measure veillance flux from cameras, microphones, and other manmade sensors. The difficulty in measuring biological veillance flux stemmed from the difficulty in tapping into the optic nerve, if one wishes to duplicate the same veillametric methods used to measure cameras' ability-to-see. As a result, a new method is required.

We will first review the fundamental veillametrics algorithms for manmade cameras and optical sensors.

Veillance flux "emitted" by manmade cameras is measured by tapping into the output signal of the camera, then optically stimulating the physical space surrounding the camera in two or three dimensions, and finally feeding the results into a veillametric algorithm [1] to compute the amount of information that can be sensed in each region of space — that is, the amount of independent veillance flux falling on each location.

Other methods exist which do not strictly measure veillance flux, but which give an approximate location of the field-of-view of a camera:

- Coupling the camera with an infrared (or other invisible) light source, and measuring locations where that infrared light is received [2], [4];

- Connecting the camera's output through an uncontrolled positive feedback loop to control a light bulb, which glows more brightly when it is inside the field of view of a camera [4] (i.e. this method indicates the boundaries of the camera's field of view).

The flaw in both of these methods is that they cannot distinguish the amount of information-sensitivity transfer though space, i.e. veillance flux. For example, when the "ability-to-see" reflects off a white rough surface, the resulting loss in unique veillance flux is detected by a true veillametric sensing algorithm [1], whereas the coupling method and feedback method merely measure the decay pattern of energetic light transmission and reflection.

After it is measured, veillance flux at every point in space can be computationally rendered as a map [2], or can be viewed in real-time augmented reality (AR) [3], or can be rendered onto the 3D physical world with controlled light sources [4], [2] and long-exposure photography (abakography) [5].

The veillance flux data can also be displayed without graphic rendering, in a veillance dosimeter [2]. This device is analogous to a radiation dosimeter [6] as used in the nuclear industry, as a body-worn patch or device to integrate total radiation dose over a period of time. However, the veillance dosimeter is sensitive to the sensitivity to radiation. That is,

it measures how much a person is being photographed or otherwise sensed. It therefore measures information-bearing reverse optics, or *extramissive optics*.

To explain numerical veillance measurement, we now explore a formulation of information-bearing extramissive optics.

III. BACKGROUND: EXTRAMISSIVE RADIATION, VS. INTROMISSIVE RADIATION

Figure 2 shows two complementary types of radiation: the propagation of light, versus the propagation of the *sensitivity to light* through space. The veillance field and veillance flux, introduced in [1], are drawn in Fig. 2. Unlike light propagation, the veillance field and veillance flux indicate the *information-bearing capacity* of light rays traced in reverse.

Radiation, whether emitted by a light source, or emitted by a camera, follows a $1/r^2$ decay pattern if is emitted radially. That is, the power intensity of light decreases as $1/r^2$ relative to distance r from a point source. Similarly, veillance flux density decays with distance as $1/r^2$ (in the limit of a small aperture approaching a pinhole camera) [2]. The reason for the latter is the spreading of the cross-sectional area of *vixels* [1], the spatial regions controlling each linearly independent pixel, shown in Fig. 2.

This dual inverse-square law has the interesting effect that if a radiative power source, such as a pulse-coded infrared source, is coupled to a camera, then a poor-quality veillance flux probe can be built using a handheld optical sensor, detecting veillance flux density in proportion to the infrared power received [2]. However, this method is inaccurate if the optical environment creates vixel degeneracy [1], as illustrated in Fig. 3b and Fig. 2. It also does not account for the nonlinear effects of camera saturation. An optical stimulation method (e.g. using LASERs or LED arrays to stimulate regions of space to test for veillance flux “arriving” from a sensor), and a veillance degeneracy analysis algorithm [1], better account for loss of linear independence as veillance reflects and scatters in a complex optical environment. Measuring the capacity-to-sense over a region of space leads to the veillance field and veillance flux [1] as follows.

The *veillence vector field*, \vec{V} , was defined as a vector field everywhere pointing in the direction of veillance radiation, and with its magnitude equal to the density of vixels (spatial region controlling one pixel) [1]. The veillance vector field represents the spatial behavior of the ability-to-see. It can further be generalized as a vector set field for spatial regions where veillance rays intersect.

Veillance flux, Φ_V , describes the veillance radiation impinging a surface, Ψ , integrated over infinitesimal segment normals $d\vec{S}$ at positions \vec{r} :

$$\Phi_V = \int_{\Psi} \vec{V}(\vec{r}) \cdot d\vec{S} \quad (1)$$

The *veillence field* can be expressed as:

$$V(\vec{r}, \angle \vec{\chi}, d) = V(x, y, z, \theta, \phi, d) \quad (2)$$

and is a scalar quantity that accounts for intersecting veillance rays from multiple pathways (direction $\vec{\chi}$ or angles θ and ϕ),

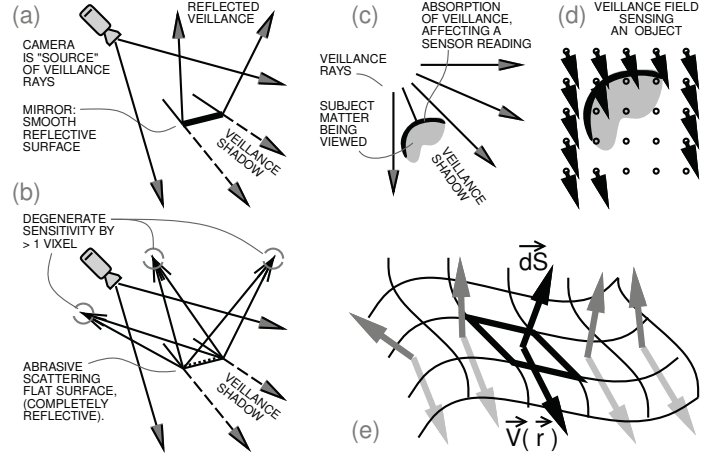


Fig. 3. Veillametric diagrams, to show the Ability-to-See propagating through space: **(a) Reflection** of veillance rays, and a *veillence shadow*. **(b) Degeneracy** in reflected veillance: Even if all *light* is reflected, not necessarily all unique *veillence* is reflected. For example, a perfectly white, yet diffusely-reflective surface, can cause a reduction in reflected veillance flux, resulting from a loss of uniqueness of each pixel. That is, a white rough-textured (“blurry”) object can *absorb* veillance even if it reflects all light, because it does not uniquely reflect as a mirror does. This example shows that energetic optics and veillance optics are not simply converse equivalents, or time-reversed duals of each other. **(c) Absorption of veillance** on the leading edge of an opaque object. A rough-surfaced reflective opaque object is an effective veillance absorber, because its diffused reflectance causes degeneracy in the reflected vixel rays. That is, from a sensor’s perspective it is unclear what is the content of any subject matter seen in the reflection (other than the fact that the subject matter may be getting brighter or dimmer in total); hence the reduction in veillance (*i.e.* absorption of veillance) caused by diffused reflection of light. **(d) Veillance vector field**. The veillance vector field is defined at multiple points in space, (*i.e.* a field of vectors), as opposed to vixel rays (c) which simply trace out a tangent to propagation of the sensitivity-to-light. Veillance field intensity at each point is proportional to the density of vixel rays (akin to the density of electric or magnetic field lines, forming a field intensity). **(e) Veillance flux**: Veillance impinging a more complex surface, broken down element-by-element, where the veillance vector field is integrated over the surface to yield veillance flux.

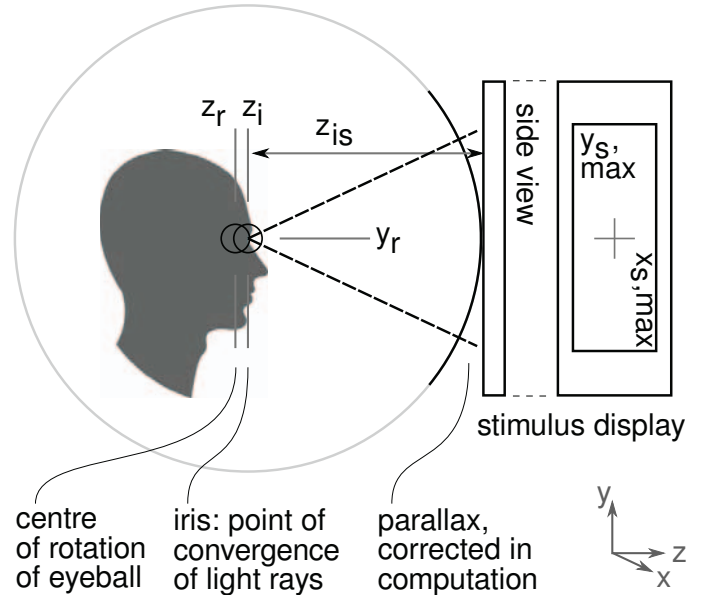


Fig. 4. Eye testing geometry to determine a 3D veillance flux map. Optical stimuli are generated in the (x, y) plane, at a distance z_{is} away from the iris, and converted to polar coordinates to compensate for parallax and radial flux decay ($1/r^2$) of veillance flux.

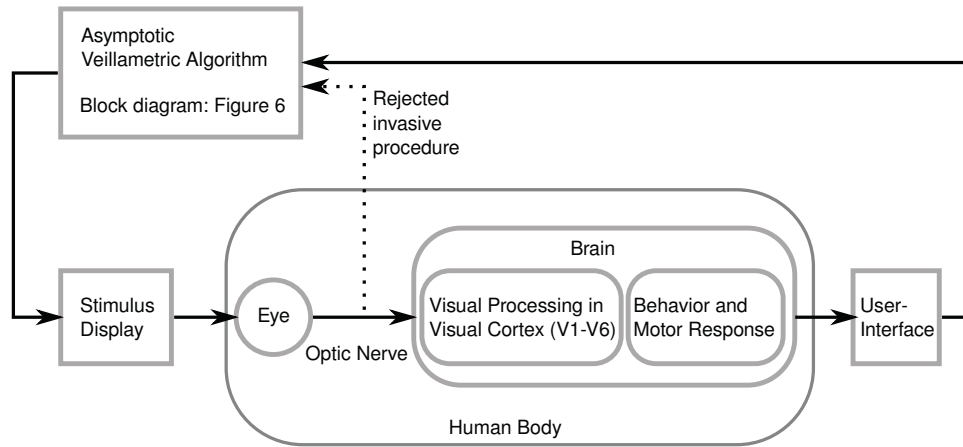


Fig. 5. Bio-Veillametrics measurement and testing: signal flowpath. To create a 3D map of the sensitivity-to-light as it propagates through space, we must query the level of human perception, and relate it to how that perception propagates through space. This signal loop is more than merely a feedback loop of brightness or strength of a received signal. Instead, the veillance flux measurement continually adapts to the responses received, and chooses the next stimulus to anticipate an optimal future test, where the veillance flux measurement is adjusted over finer and finer increments of precision. The result is an asymptotic measurement of dynamically changing veillance flux, which can vary in response to the individual's activity and attention paid to different parts of his or her visual field.

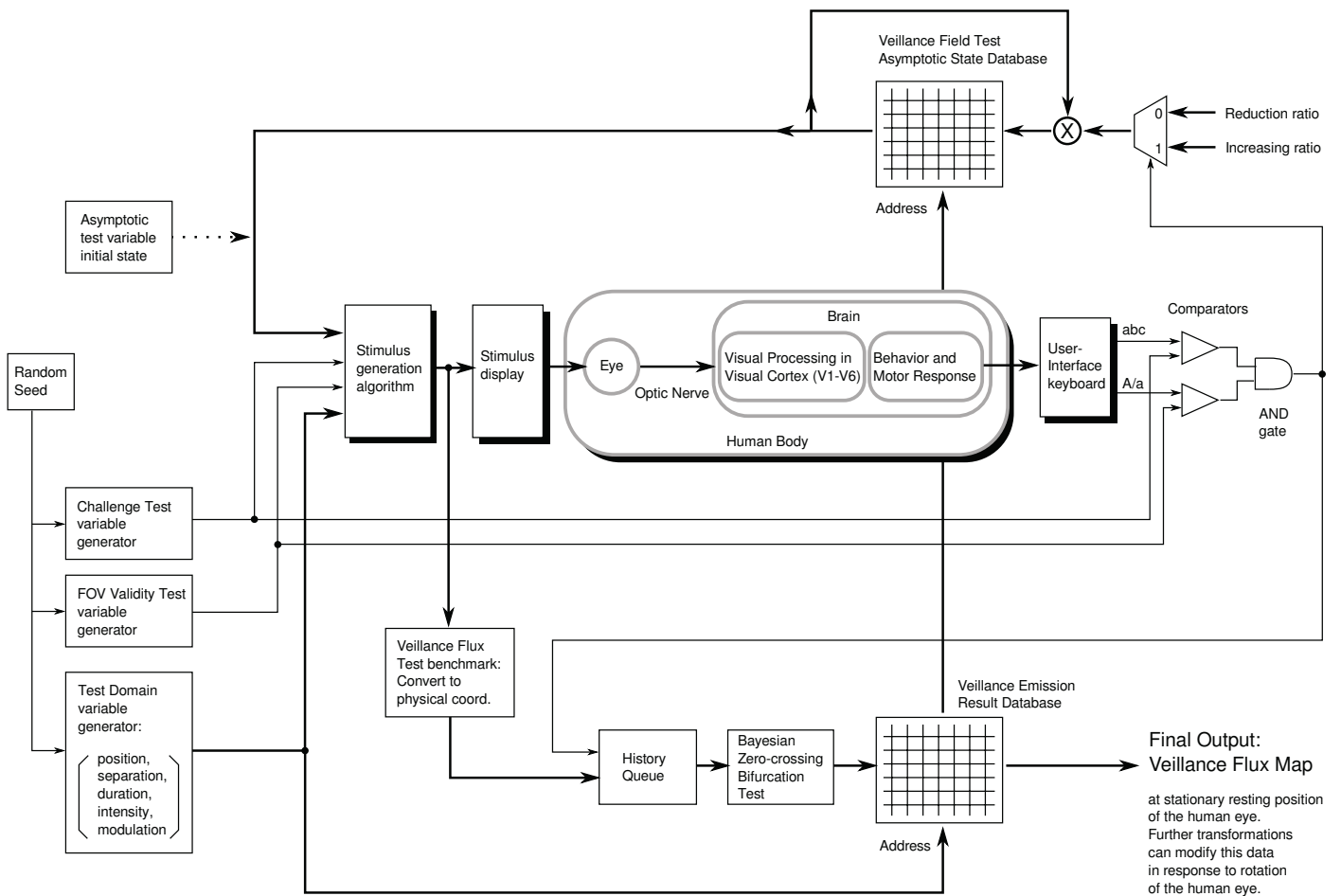


Fig. 6. Asymptotic testing process block diagram, to measure veillance flux “emitted” by human eyes and transmitted to locations throughout a 3D space. The stimulus display can be placed anywhere in that 3D space to test veillance flux at any location, but we typically place the stimulus display in front of the human test subject with a known geometry, to be able to extrapolate veillance flux measurements elsewhere throughout a room or virtual space.

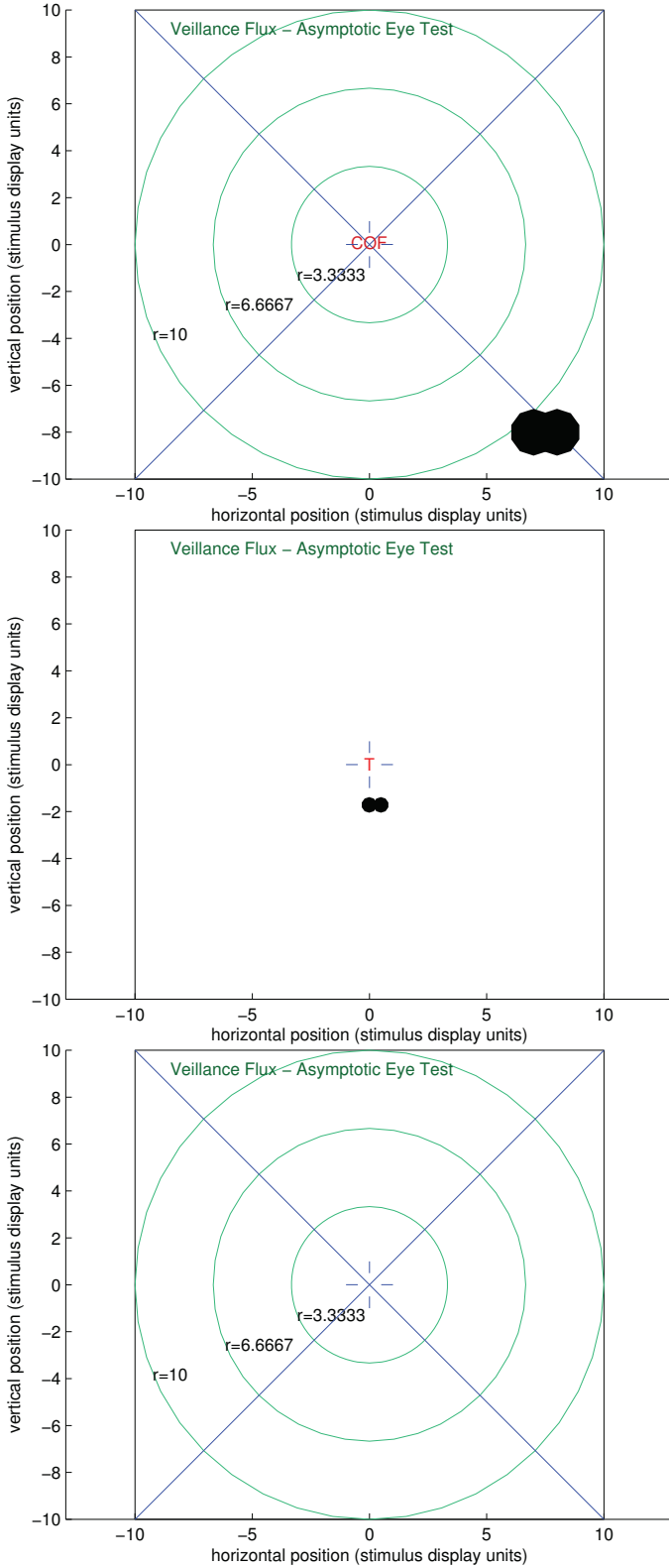


Fig. 7. Testing process: view of the stimulation display, shown on a computer monitor positioned in front of a test subject. (a) Initial graphics for alignment. (b) Stimulus group, flashed for a fraction of a second, with specific parameters for each test (challenge state, flux bifurcation difficulty, and position), as well as alignment challenge symbol (red color), also flashed for a fraction of a second. (c) Ground-state display immediately after the stimulus, when the test subject is asked to respond.

and from multiple sensor devices (d). V is an information-bearing analogue of the 5D plenoptic function. V can be measured in $[\text{vixels}/\text{sr}/\text{m}^2]$, and its bit-rate sister quantity ∇ is measured in $[\text{bits}/\text{sr}/\text{m}^2/\text{s}]$. The intensity of the ∇ field indicates the bit rate of information sensitivity, per steradian, per unit area. A veillance dosimeter [2] gives an accumulating dose reading, measured in $[\text{bits}]$, by aggregating ∇ over a macroscopic area and solid angle, and integrating over time.

IV. BIOLOGICAL FEEDBACK LOOPS FOR VEILLANCE MEASUREMENT AND VISUALIZATION

A. Background on biological vision processing

We will describe the first measurements of human-eye veillance flux, which differs greatly from the orderly arrangement of veillance flux as emitted by cameras. To measure and track the eye's ability-to-see in space, we required a new process sensitive to the human visual system.

The human visual system is made up of the eyes, optic nerves, visual cortex, and selected other regions of the brain.

Veillance flux concentration is dominated by a high retinal receptor concentration in the center of the field of view, but is also affected by processing in the visual cortex. The visual cortex is made of several components (repeated on each side of the brain, one for each eye):

- V1 (Primary Visual Cortex): edge detection, spatial frequency and color discrimination [7], [8]
- V2: orientation, contours, color, spatial frequency; figure *v.s.* ground, object recognition memory (ORM) [9], [10]
- V3: coherent motion of patterns; global motion [11]
- V4: first area which is modulated by selective attention; encodes salience, has long-term plasticity; intermediate complexity of object features (geometric shapes but not faces) [12]
- V5 (MT): motion (speed and direction) of objects; eye-movement guidance [13], [14], [15]
- V6 (DM): motion of the self; works by identifying very broad lines and contours across the entire visual field [16], [15]

We will test veillance flux concentration based on an individual's ability to discriminate the density of stimuli in 3D space. Since we test a response through human behavior, we automatically factor in both the eyes' and visual cortex response of visual processing (as in Fig. 5).

B. Eye test process

Before veillance flux can be rendered and displayed, an individual's veillance flux must be measured.

The test subject is positioned in front of a stimulus display, facing the display at its center (Fig. 4). The subject is told to gaze at center marker crosshairs on the display (Fig. 7). Optical stimuli are generated in the (x, y) plane, at a distance z_{is} away from the iris, and converted to polar coordinates to compensate for parallax and radial decay ($1/r^2$) of veillance flux.

The stimulus display contains a graphical area and a text area where instructions are displayed. The text first shows instructions:

```
Keep your eyes directed at the center markers.
The system will test to determine if your
eyes have been properly positioned.
Please respond honestly, to speed up the test.
(Note that the test overcomes dishonest
responses gradually over a longer duration).
```

```
In response to each stimulus, type a letter
that corresponds to the letter you see
inside the crosshairs.
Type a capital letter
  if you see the "strong" stimulus
  elsewhere on the display.
Type a lower-case letter
  if you see the "weak" stimulus
  elsewhere on the display.
```

When ready to begin, press ENTER.

The graphical display shows a calibration pattern initially (Fig. 7a) until the user presses ENTER.

When the test begins, two sets of symbols are momentarily flashed for a period of 0.2 seconds (e.g. Fig. 7b). The two symbols are: an alphanumeric character to test whether the eyes are aligned properly (otherwise that particular test segment is invalidated), and a group of shapes in the optical field (the stimulus group).

The stimulus group is randomized from a set of challenge states: The challenge state space, \underline{c} , is either:

- varying brightness or alpha value; or
- varying quantities of stimulus symbols positioned in close proximity.

The challenge state is randomized for each test, to overcome honest/dishonest responses from the individual being tested, and to provide an honest indication of the individual's resolving power at those particular stimulus parameters.

The stimulus group's other randomized parameters are:

- varying size and shape, \underline{d} , to provide a ground truth to determine whether the veillance flux measurement goes up or down; The algorithm increments to an **easier** stimulus \underline{d} if the user is incorrect or unable to visually distinguish the previous stimulus. On the other hand, the algorithm increments to a more **difficult** stimulus \underline{d} if the user correctly identifies the previous stimulus.
- varying position in the optical field, \vec{r} , to measure veillance flux at all locations.

The stimulus group is therefore flashed with parameters $(\underline{c}, \underline{d}, \vec{r})$, to simultaneously execute all of these test requirements. The alignment challenge symbol \underline{a} is also flashed at the same time, to determine whether the eyes are directed at it at the same time as the stimulus group – this validates position \vec{r} and ensures the correct amount of veillance flux is measured for that location without cheating.

The user is asked to respond on a user-interface keyboard (keeping hands on it without looking down), with keypresses to respond with their best guess of the parameters $(\underline{a}, \underline{c})$.

Even if dishonest responses are given, and the individual could not in fact see the difference in the stimulus group but still got the correct

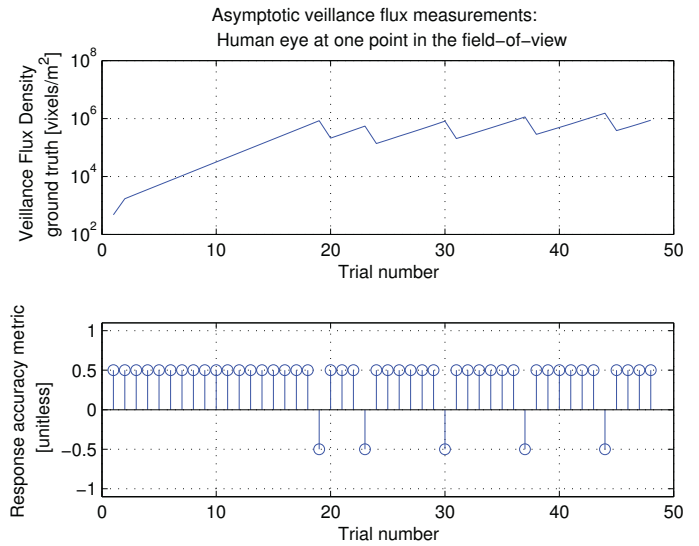


Fig. 8. Time-evolving measurement of veillance flux, at one single location in the eye's field of view. The human test subject's response accuracy is shown as a sequence of positive and negative values, plotted in the second graph. Each response, in each segment of time, governs the next test stimulus presented in the next segment of time..

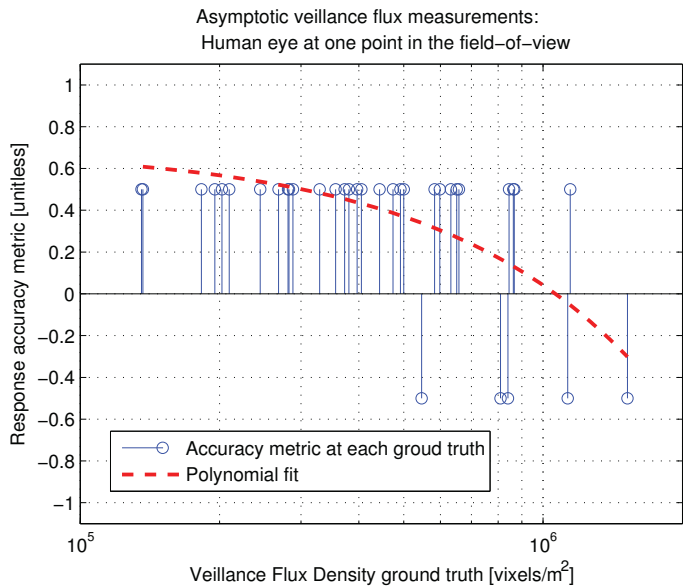


Fig. 9. Asymptotic measurement of veillance flux at a single location in the eye's field of view. In this histogram-like display of data, the value to be measured is placed in the domain (horizontal axis) and evaluated in terms of human eyesight response accuracy. Polynomial regression allows an estimation of veillance flux at the zero-crossing (i.e. the bifurcation between correct sight of the stimulus and incorrect sight of the stimulus).

answer by guessing, then due to the randomized $(\underline{c}, \underline{d})$ the algorithm will still converge toward a true measurement of veillance flux for that spatial position. An honest keypress-code is also provided: If the user wishes to honestly admit that he/she could not distinguish the stimulus, then by pressing '0', he/she allows the algorithm to directly increment the stimulus to an easier state of \underline{d} , thus approaching more quickly toward a measurement of veillance flux at that position.

The 2D or 3D space is traversed by \vec{r} , and for each position a sequence of stimuli converge toward a measurement of veillance flux for that position.

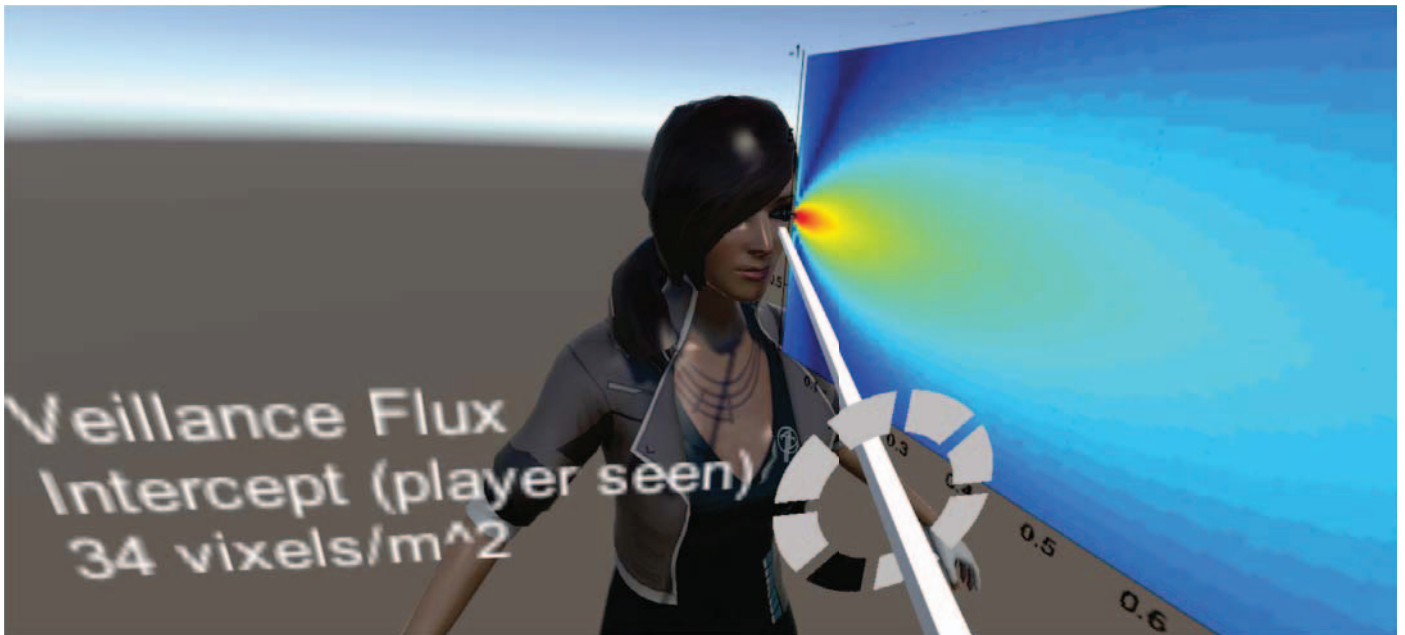


Fig. 10. Game environment in Unity3D, rendering in 3D with imported veillance field extending a certain distance away from an avatar. 3D interaction can also include: (1) calculating the veillance field at distant fixed objects, to determine if they are seen, and to what extent; (2) overlaying a 3D environment on the real world while wearing augmented-reality (AR) glasses, to visualize human veillance in real-time.

V. DYNAMIC VEILLANCE FIELDS, AND ASYMPTOTIC MEASUREMENTS

A 3D map of veillance flux is time-varying if it is “emitted” from a time-varying sensing process. For example, a camera may have a constant resolution, but if it broadcasts a time-varying number of pixels, then the 3D veillance flux emitted from the camera is time-varying (when measured *with respect to the broadcast process*). Similarly, although an eye has a given number of receptor cells, the eye’s veillance flux is affected by the amount of visual information actually used by the visual cortex. If a visual distraction such as motion occurs off to the side of the field of view, the effective veillance flux tested in front of the eyes may be reduced if conscious focus changes. As well, dynamic ranges of retinal rods and cones lead to better or poorer responses to different lighting levels, and thus as lighting levels vary, this is mapped to a variation in visual precision, and thus to time-varying changes in veillance flux. Our time-evolving testing system is designed to create time-varying maps of veillance flux, or alternatively to create static maps of veillance flux (whose data points evolve starting with fast, coarse measurements and converge towards fine precise measurements). This was accomplished with an asymptotic test behavior which starts with initial testing parameters and gradually approaches a final veillance flux map, via a feedback loop between human and testing system.

This asymptotic testing system, seen in Figs. 5 and 6, is more than merely a feedback loop responding to the brightness or strength of a received signal. Instead, the veillance flux measurement continually adapts to the response accuracy and the stimulus spatial density, and chooses the next stimulus to anticipate an optimal future test to bifurcate the next veillance flux measurement with the greatest precision.

Randomized positions are computed for stimuli to appear in the display (Fig. 7). Despite a random “snow” appearance of the stimuli, the asymptotic measurement behavior continually updates veillance flux measurements at each position, while avoiding biases that may have emerged if adjacent locations had been tested in sequence (*i.e.* suggesting to the test subject where to expect the next stimulus).

Asymptotic behavior of a static test, for one location, can be seen in Fig. 8. This data is combined in Fig. 9, where a zero-crossing point between equally-likely false and true results for \underline{c} reveals the estimate of veillance flux at one position.

VI. RENDERING BIOLOGICAL VEILLANCE FLUX

An example of the resulting veillance flux is shown in Fig. 11. This graph is a 2D slice of the veillance flux, normalized and mapped to a logarithmic color space.

The measurements can be rendered graphically on the same spatial coordinates as a photograph or video of a human body itself. See Fig. 1. This is ideally suited to augmented-reality environments, where one individual (A) looks through display glasses and sees another individual (B), as viewed in Fig. 1. A’s glasses can render and overlay veillance flux coming out of B’s eyes, based on an earlier measurement of B’s personal veillance flux.

The mathematical results can also be moved into a 3D rendering environment such as Unity3D (Fig. 10). Comparing Fig. 1 to Figs. 10 and 11 reveals two different rendering techniques. The first technique in Fig. 1 is a vector-based rendering of colored polygons, which removes information about the decay of veillance as it radiates and spreads out. The second technique is a raster-style rendering, where flux is rendered for each 2D pixel or 3D voxel.

We note that these sight maps are measured relative to the anterior/posterior (front-back) axis of the eyeball itself. As the eye gaze rotates up/down or side to side, the veillance flux moves with it, and can be re-rendered as in Fig. 11. We can either ignore small physical truncations caused by the nose, cheeks and eyebrows, and gaze-angle-dependent changes to visual-cortex processing, or we can re-test veillance flux at each different gaze angle.

Future work will use eye-tracking hardware and software to enable real-time efficient rendering of veillance flux. The measured veillance field will be dynamically moved and rotated in response to a human walking and looking in different directions over time. This real-time solution will save the difficulty of repeating the measurements each time an individual moves.

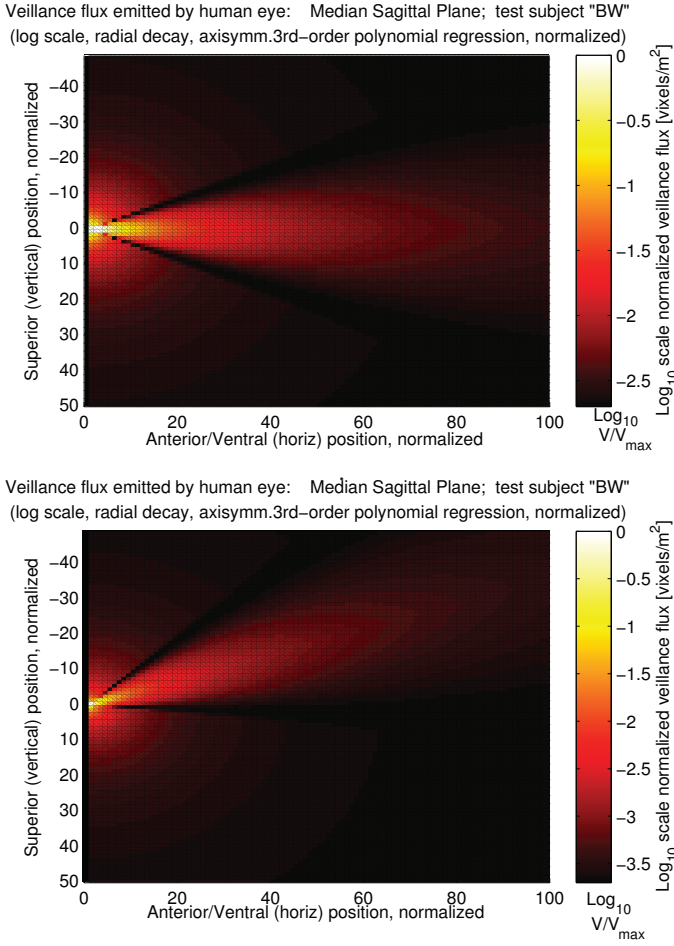


Fig. 11. Veillance flux emitted by a human eye, experimentally measured. The iris of the eye is located at position (0,0) of this slice in the vertical plane. When the eye looks up, the pattern changes (second plot: 20-degree angle). Veillance flux has been normalized and mapped to a logarithmic color space. The veillance flux along the center line of the field of view is much stronger than it appears, due to the log-scale color map. The veillance flux density peaks in the iris (0,0) where the rays of veillance converge and diverge, but for diagram clarity this rendering does not show the high-density peak exactly at (0,0). In the extreme case, veillance flux density would be infinite in a theoretical case of an infinitely-small pinhole camera iris opening. (These normalized plots appear the same at any length scaling, since the normalized veillance flux density scales inversely as normalized distance scales larger. Note also that the narrow black bands are caused by a polynomial smoothing function.)

VII. APPLICATIONS OF MAPPING SIGHT

Maps of veillance flux lead to several applications. By measuring veillance flux, we determine level of visual acuity/awareness throughout 3D space, beyond simple gaze-tracking (which only reveals a small set of numbers indicating the angle of viewing).

Camera coverage in a room, or eyesight attention to displays, warning messages, signs, and advertisements, can all be represented with veillance flux. An intricate map of “sight” falling on an advertisement, or on a control panel, enables marketing research, industrial operations research, and health science research.

A new type of eye test is created by this work. While ordinary eye tests give a small set of numbers describing the ability to focus, veillance flux creates a large array of numbers intricately describing sight manifested over 3D space.

In a gaming scenario, individuals can gain points when they see another player, or lose points when they are seen. This can occur in a physical environment with augmented-reality hardware, or a virtual game environment (e.g. Fig. 10). Conversely, in a “Medusa” scenario, players could lose points when they see another player, or when the players mutually see each other.

The advantage of biological veillance flux is that it measures more than merely a binary value of whether or not something is seen. It further measures the *degree* to which an individual sees material in each location, integrated over space and time, to provide a richly complex time-varying metric of how much “sight” or “veillance” falls on another object, person, or scene.

VIII. VEILLANCE FLUX STANDARDS

The ability to map the sensory “emissions” of an eye (or other sensor) allows us to determine the overall amount of veillance flux falling on a target, such as on a roadway (in the case of a driver), on a control panel (in the case of a nuclear power plant worker), or on a room or hallway (in the case of a security camera). Indeed we can create standards to regulate this.

We can specify minimum levels of veillance flux required at all times; for example, a required minimum amount of attention paid to each part of a control panel by an aviation pilot. Security cameras in a building could have standards for camera coverage, to qualify for reduced insurance rates.

To create veillance flux standards, we use a Range Density Function (RDF) [17] of veillance flux density throughout a space.

The Range Density Function (RDF) [17] is a continuous version of a histogram, and is a deterministic (non-random) analogue to the Probability Density Function (PDF). The RDF assigns weights to each quantity-level based on that quantity’s population or abundance, *i.e.* in the *range* of the quantity or function being measured (veillance flux density) as opposed to the *domain* (reminiscent of a Lebesgue integral versus a Riemann integral). The RDF has key features: 1. Describes physical reality deterministically, rather than probabilistically as with a PDF; 2. Defined for all possible ranges of a quantity, from $-\infty$ to $+\infty$; 3. Normalized so it integrates to 1: $\int_{-\infty}^{\infty} R_V(q)dq = 1$.

The *veillance RDF* can be determined by mapping veillance flux in a 3D space, and then computing histograms, approached in the limit with asymptotically increasing histogram resolution. Each bin of a histogram (between quantities a and b) is related to the RDF as follows:

$$\begin{aligned} \int_a^b R_V(q)dq &= \text{Histogram } [a \leq V(\vec{r}) \leq b] \\ &= \frac{1}{X} \int_X \left[\begin{matrix} u(V(\vec{r})-a) \\ \cdot \\ u(b-V(\vec{r})) \end{matrix} \right] \cdot dX_{\vec{r}} \end{aligned} \quad (3)$$

where $u(\cdot)$ is the Heaviside step function, and an RDF is found by observing veillance $V(\vec{r})$ at each volume segment $dX_{\vec{r}}$ in space X .

We can then create bounds on the veillance RDF. See Fig. 12. The simplest standard specifies that all veillance flux must be greater than or less than a minimum or maximum throughout all the space. More generally, a veillance standard has a set of constraints:

$$C_L = \begin{bmatrix} V_{L1} & R_{V,L1} \\ V_{L2} & R_{V,L2} \\ \vdots & \vdots \\ V_{L\eta} & R_{V,L\eta} \end{bmatrix}, \quad C_H = \begin{bmatrix} V_{H1} & R_{V,H1} \\ V_{H2} & R_{V,H2} \\ \vdots & \vdots \\ V_{H\mu} & R_{V,H\mu} \end{bmatrix} \quad (4)$$

with η constraints on low values of veillance, forcing spatial regions having less veillance than $V_{L\eta}$ to be less populous than $R_{V,L\eta}$, as well as μ similar constraints on high values of veillance. One elementary case, using $V_{L1} > 0$, $R_{V,L1} = 0$, $\eta = 1$, $\mu = 0$ is shown in Fig. 12,

Sensory Histogram: Limits on sensing required in a room, street, vehicle, or other 2D/3D space.

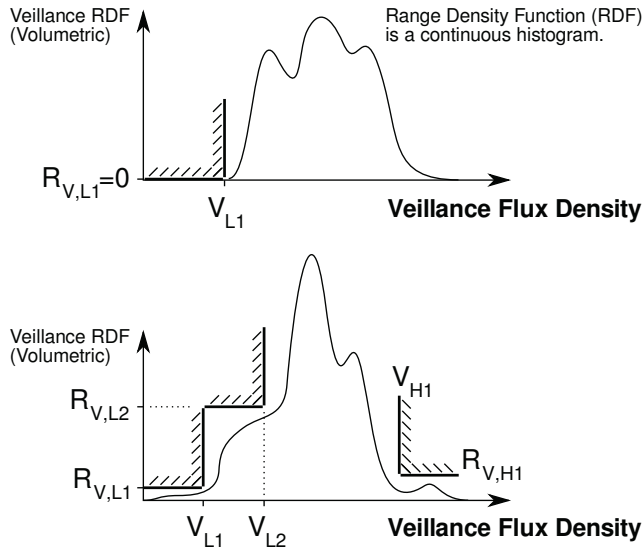


Fig. 12. Sensory standards, to specify minimum and maximum amounts of sensing (eyesight, camera sight, etc.) required, for safety standards, or security standards, or privacy standards.

along with a more sophisticated case which allows small areas of low veillance, and further constrains areas of high veillance. Applied to security cameras, for example, this creates allowances for small locations where veillance is blocked, or locations near a camera lens with high resolution.

These standards essentially put a limit on high-resolution sensing (e.g. maximum camera coverage for **privacy**), and limit areas with low-resolution (e.g. minimum camera coverage for **safety**).

Safety standards for eyesight falling on critical control panels, such as in transportation or industrial plants, could also have minimum veillance flux for each location over time, to ensure important warnings are not missed. Ensuring drivers, pilots and captains look ahead can also be enforced with precise veillance flux standards.

IX. CONCLUSION

We have implemented a system to measure and display veillance flux from human eyes, for the first time, which represents the “ability to see” moving through space. Veillance flux is emitted by human eyes according to the density of sensitivity-to-information, and propagates away from the eyes throughout space.

Applications include: medical diagnostics (as a new type of eye test), industrial safety (measuring human sight falling on control panels, or on the road ahead from a driver’s eyes), and marketing research (measuring human sight falling on signs or advertisements).

Biological veillance flux opens up a new world of sensing itself—veillametrics. More than merely a binary value of whether or not something is seen, it further measures the *degree* to which an individual sees various objects, integrated over space and time, to provide a richly complex time-varying metric of how much “sight” or “veillance” falls on an object, person, or scene.

X. ONLINE INFORMATION

Further information and demonstrations are available at:
<http://veillametrics.com>

REFERENCES

- [1] R. Janzen and S. Mann, “Veillance flux, vixels, veillons: An information-bearing extramissive formulation of sensing, to measure surveillance and sousveillance,” *Proc. IEEE CCECE*, May 4-7 2014, 10 pages.
- [2] —, “Veillance dosimeter, inspired by body-worn radiation dosimeters, to measure exposure to inverse light,” *Proc. IEEE GEM*, pp. 267–9, 2014.
- [3] R. Janzen, S. N. Yasrebi, A. J. Bose, A. Subramanian, and S. Mann, “Walking through sight: Seeing the ability to see, in a 3-D augmented reality environment,” *Proc. IEEE GEM*, pp. 313–4, 2014.
- [4] S. Mann, R. Janzen, S. Feiner, J. Hansen, S. Harner, S. Baldassi, and M. A. Ali, “Wearable computing, 3d augmented reality, photographic/videographic gesture sensing, and veillance,” in *Proc. ACM Tangible and Embedded Interaction (TEI2015)*, 2015, pp. 497–500.
- [5] S. Mann, R. Janzen, T. Ai, S. N. Yasrebi, J. Kawwa, and M. A. Ali, “Toposculting: Computational lightpainting and wearable computational photography for abakographic user interfaces,” in *Proceedings of the IEEE CCECE*. IEEE, 2014.
- [6] L. Pardue, N. Goldstein, and E. Wollan, “Photographic film as a pocket radiation dosimeter,” *Atomic en: bioph, biol, med*, vol. 1, no. 5, p. 169, 1948.
- [7] K. Foster, J. P. Gaska, M. Nagler, and D. Pollen, “Spatial and temporal frequency selectivity of neurones in visual cortical areas V1 and V2 of the macaque monkey,” *The Journal of Physiology*, vol. 365, no. 1, pp. 331–363, 1985.
- [8] M. Stevens and I. C. Cuthill, “Disruptive coloration, crypsis and edge detection in early visual processing,” *Proceedings of the Royal Society of London B: Biological Sciences*, vol. 273, no. 1598, pp. 2141–2147, 2006.
- [9] D. Y. Ts’o, M. Zarella, and G. Burkitt, “Whither the hypercolumn?” *The Journal of Physiology*, vol. 587, no. 12, pp. 2791–2805, 2009.
- [10] M. F. López-Aranda, J. F. López-Téllez, I. Navarro-Lobato, M. Masmudi-Martín, A. Gutiérrez, and Z. U. Khan, “Role of layer 6 of V2 visual cortex in object-recognition memory,” *Science*, vol. 325, no. 5936, pp. 87–89, 2009.
- [11] O. Braddick *et al.*, “Brain areas sensitive to coherent visual motion,” *Perception*, vol. 30, no. 1, pp. 61–72, 2001.
- [12] J. Moran and R. Desimone, “Selective attention gates visual processing in the extrastriate cortex,” *Science*, vol. 229, no. 4715, pp. 782–784, 1985.
- [13] R. T. Born and D. C. Bradley, “Structure and function of visual area MT,” *Annu. Rev. Neurosci.*, vol. 28, pp. 157–189, 2005.
- [14] J. H. Maunsell and D. C. Van Essen, “Functional properties of neurons in middle temporal visual area of the macaque monkey. I. selectivity for stimulus direction, speed, and orientation,” *Journal of neurophysiology*, vol. 49, no. 5, pp. 1127–1147, 1983.
- [15] J. F. Baker, S. E. Petersen, W. T. Newsome, and J. M. Allman, “Visual response properties of neurons in four extrastriate visual areas of the owl monkey (*Aotus trivirgatus*): a quantitative comparison of medial, dorsomedial, dorsolateral, and middle temporal areas,” *Journal of Neurophysiology*, vol. 45, no. 3, pp. 397–416, 1981.
- [16] V. Cardin and A. T. Smith, “Sensitivity of human visual and vestibular cortical regions to egomotion-compatible visual stimulation,” *Cerebral Cortex*, vol. 20, no. 8, pp. 1964–1973, 2009.
- [17] R. Janzen and S. Mann, “High dynamic range simultaneous signal compositing, applied to audio,” in *Proc. IEEE CCECE 2012, Montreal*, April 29 to May 2 2012.